

Research Paper

Zernike Moments Description of Solar and Astronomical Features: Python Code

Hossein Safari¹ · Nasibe Alipour^{*2} · Hamed Ghaderi³ · Pardis Garavand⁴

¹ Department of Physics, Faculty of Science, University of Zanjan, University Blvd., Zanjan, 45371–38791, Iran;

email: sfari@znu.ac.ir

² Department of Physics, University of Guilan, Rasht, 41335–1914, Iran;

*email: nasibealipour@gmail.com

³ Department of Physics, Faculty of Science, University of Zanjan, University Blvd., Zanjan, 45371–38791, Iran;

email: albert.ghaderi@gmail.com

⁴ Department of Physics, Faculty of Science, University of Zanjan, University Blvd., Zanjan, 45371–38791, Iran;

email: pardisegaravand@gmail.com

Received: 26 August 2023; **Accepted:** 19 November 2023; **Published:** 27 November 2023

Abstract. Due to the massive increase in astronomical images (such as James Web, Solar Dynamic Observatory, and Solar Orbiter), automatic image description is essential for solar and astronomical. Zernike moments (ZMs) are unique due to the orthogonality and completeness of Zernike polynomials (ZPs); hence, ZMs are valuable for converting a two-dimensional image to a one-dimensional series of complex numbers. The magnitude of ZMs is rotation invariant, and by applying image normalization, scale and translation invariants can be made, which are helpful properties for describing solar and astronomical images. The lower-order ZMs express the overall shape of the objects of an image, and the higher-order ZMs provide more details of the objects and delicate structures within an image. In this Python package, available at GitHub and PyPI, we describe the characteristics of ZMs via several examples of solar (large and small scale) features, astronomical, and human face images. These independent and unique properties of ZMs can describe the structure and morphology of objects in an image. Hence, ZMs are helpful in machine learning to identify and track the features of several.

Keywords: Zernike moment, Solar images, Python code

1 Introduction

Objects recognition in images has been developed in several disciplines [1–6]. Recently, feature extraction for machine learning of object finding and tracking based on image moments was investigated [7]. Moments are a class of image description [8,9]. Since the image data of various fields such as biology, medicine, optics, astronomy, and solar physics are vastly recorded, these images' descriptions are out of manual analysis. The image moments are quantities that describe an image's shape, objects, and structure.

* *Corresponding author*

This is an open access article under the **CC BY** license.



Zernike moments (ZMs) map an image to a complex number series [10–15]. ZMs are a family of orthogonal moments due to the property of Zernike polynomial functions [16]. Due to the exponential phase term of complex Zernike polynomials, the magnitude of ZMs is rotation invariant. In the literature, a comprehensive review of Zernike polynomials and applications were explained [17–28]. Recently, ZMs have been widely used for describing the characteristics of various digital images in different disciplines [20–28]. The ZMs, as a basis of machine learning, were applied for the identification of solar small-scale brightenings [29–32] and small-scale (mini) dimmings [33–35]. The ZMs are valuable features for classifying solar flaring and non-flaring active regions [36–38] that developed a tool of solar flare for casting.

The layout this paper is: Sections 2 and 3 describe the Zernike polynomials and Zernike moments, respectively. Section 4 provides an overview of Python code. Section 5 gives the conclusions.

2 Zernike polynomials

The ZPs are a complete set of orthogonal continuous functions in a unit disk. The even ZPs with order n and repetition m in the polar coordinate are given by

$$ZP_{pq}(r, \theta) = R_{pq}(r) \cos(q\theta), \quad (1)$$

and the odd ZPs function is defined by

$$ZP_{p-q}(r, \theta) = R_{pq}(r) \sin(q\theta), \quad (2)$$

where the radial distance in a unit circle is $0 \leq r \leq 1$ and the azimuths angle is $0 \leq \theta \leq 2\pi$. The radial polynomials for a given set of p and q are defined by

$$R_{pq}(r) = \sum_{k=0}^{\frac{p-q}{2}} \frac{(-1)^k (p-k)!}{k! \left(\frac{p+q}{2} - k\right)! \left(\frac{p-q}{2} - k\right)!} r^{p-2k}, \quad (3)$$

in which $p - q = \text{even}$ and $|q| \leq p$. The ZPs satisfy the following orthogonality property as,

$$\int_0^{2\pi} \int_0^1 V_{pq}^* V_{p'q'} r dr d\theta = \frac{\pi}{p+1} \delta_{pp'} \delta_{qq'}, \quad (4)$$

where δ indicates the Kronecker delta function and V_{pq} is the Zernike polynomials.

Figure 1 represents the radial function R_{pq} for a set of p and q in versus radial distance of polar coordinate. We observe that the radial functions increase oscillations by increasing the order number p . This property of ZPs' radial functions is one of the main reasons for applying the ZMs to describe an image in a polar coordinate.

Figure 2 displays Z_{pq} for a set of order number $p = 0, 1, 2,$ and 3 in polar coordinates. The figure shows that each Zernike polynomials have unique radial and azimuthal structures in polar coordinates. This essential characteristic of Zernike polynomials is the main reason for describing an image based on the set of complex Zernike polynomials (combination of even and odd Zernike functions in complex number plane), which maps to a unit circle.

3 Zernike Moments

The reason to describe an image by a set of functions is due to The uniqueness theorem. This theorem explains that the moments are uniquely discriminated for a given image [8].

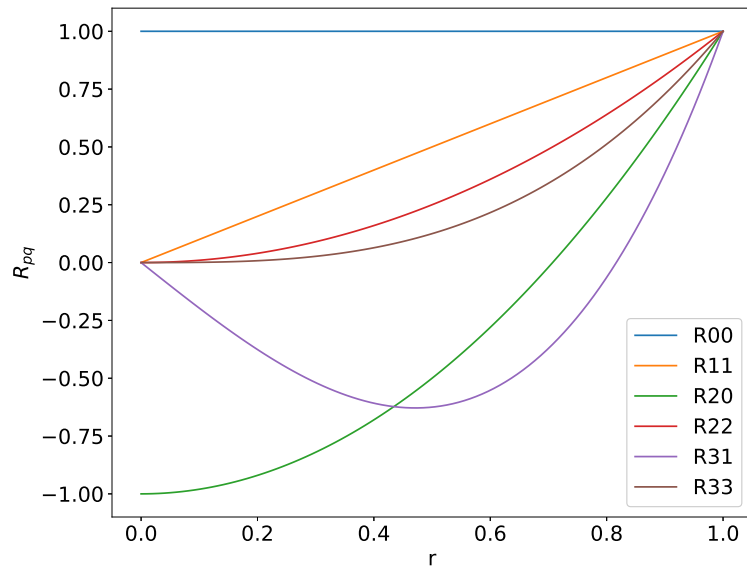


Figure 1: The radial function R_{pq} for a set of p and q in versus radial distance of polar coordinates.

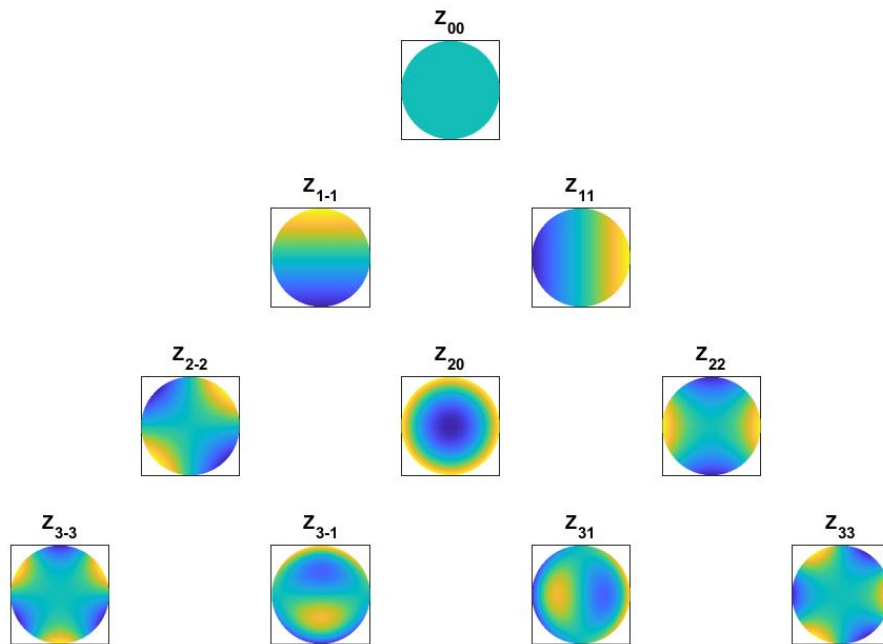


Figure 2: The Zernike polynomial Z_{pq} for a set of order number $p = 0$ (first row), $p = 1$ (second row), $p = 2$ (third row), and $p = 3$ (fourth row).

Contrariwise, we can reconstruct the original image using the set of moments. Moments can specify the properties, such as the centroid of an image, its orientation, and the geometry of the objects. Raw and central moments were defined by [8,39].

The Zernike moments (ZMs) express an image in a set of complex numbers using the Zernike polynomials $V_{pq} = ZP_{pq}(\text{even}) + iP_{pq}(\text{odd})$ [16]. The image coordinates (x, y) must be transformed into the polar coordinate. The circle's center in polar coordinates is the centroid of an image. For an image function $I(r, \theta)$, the ZM is given by,

$$Z_{pq} = \frac{p+1}{\pi} \int_0^{2\pi} \int_0^1 I(r, \theta) V_{pq}^* r dr d\theta. \quad (5)$$

For a digital image with $M \times N$ pixels, the ZMs are introduced by

$$Z_{pq} = \frac{p+1}{\pi} \sum_{i=0}^{M-1} \sum_{j=0}^{N-1} I(i, j) R_{pq}(r_{ij}) \exp(-ip\theta_{ij}), \quad (6)$$

where $r_{ij} = \sqrt{x_i^2 + y_j^2}$ and $\theta_{ij} = \arctan(\frac{y_j}{x_i})$ are the image cell mapped to a unit disk [40].

The Zernike moment array includes elements for a set of order $p=0$ to a maximum order number P_{\max} . So, the length of Zernike moments ($NZMs$) is introduced by [38]

$$NZMs = \sum_{p=0}^{P_{\max}} (p+1). \quad (7)$$

The reconstructed image (I_R) is given by an inverse transformation [41] as follow,

$$I_R(r, \theta) = \sum_{p=0}^{P_{\max}} \sum_q Z_{pq} V_{pq}(r, \theta). \quad (8)$$

Using the original and reconstructed images, we obtain the reconstruction error as

$$e^2(I, I_R) = \frac{\sum_{i=0}^{M-1} \sum_{j=0}^{N-1} (I(i, j) - I_R(i, j))^2}{\sum_{i=0}^{M-1} \sum_{j=0}^{N-1} (I(i, j))^2}. \quad (9)$$

Figure 3 shows a full disk AIA image at 171 Å inset a solar coronal bright point and the Zernike moments' maximum order 25. The Zernike moments include the imaginary and real parts (panel b). The structure of the moment series is represented by the absolute normalized Zernike moments versus labels.

Figure 4 represents an original (face) image and reconstructed images with different maximum order numbers. We observe that the reconstructed image at $P_{\max}=10$ deviated from the original image, but the reconstructed image at 45 well matched the original image. Also, increasing the maximum order number of the reconstructed image showed noisy image may be due to the discrete behavior of a digital image.

Figure 5 displays a solar active region (AR) in Solar Dynamics Observatory/Atmospheric Imaging Assembly (SDO/AIA) at 94 Å. An sigmoid event and the reconstructed images with various maximum order numbers (P_{\max}) are shown. For small $P_{\max} (< 10)$, the overall shape of the sigmoid was reconstructed. We observe that with increasing the P_{\max} , the reconstructed image approaches the original image at $P_{\max} (= 31)$. We also see that the reconstructed image deviates from the original for large $P_{\max} (= 46)$.

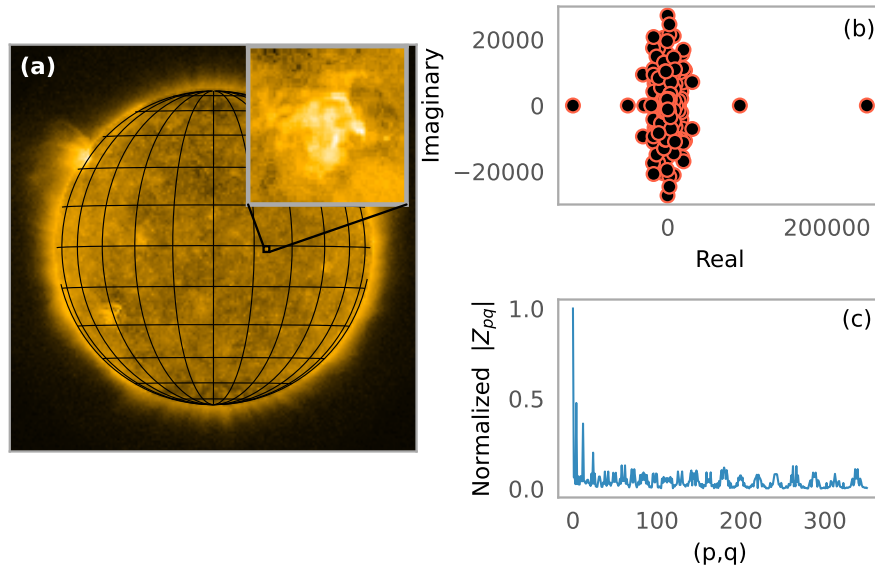


Figure 3: The full disk AIA image at 171 Å that inset a solar coronal bright point (a), the imaginary and real parts of Zernike moments for a maximum order number of 25 (b), and the absolute normalized Zernike moments versus labels (p, q) (c).

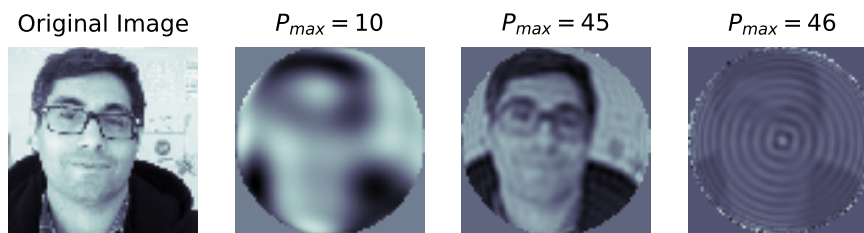


Figure 4: From left to right panels represent the original (face: Hossein Safari) image and reconstructed images with the different maximum order numbers ($P_{max} = 10, 45,$ and 46), respectively.

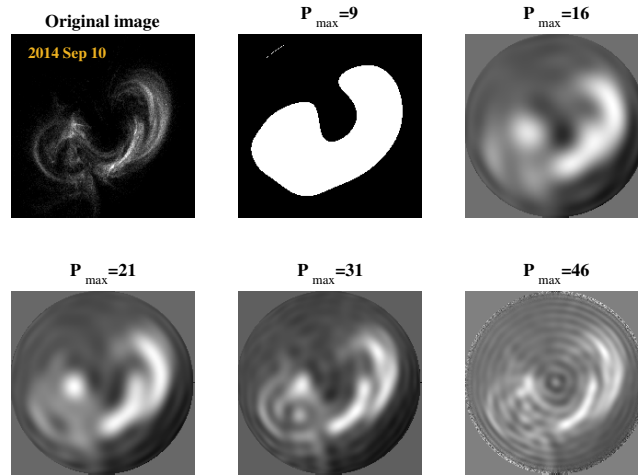


Figure 5: An active region (sigmiod: left top panel) from SDO/AIA at 94 Å. The reconstructed images for $P_{\max}=9, 16, 21, 31,$ and 46 [38].

Figure 6 shows the original and reconstructed images with the different maximum order numbers for a spiral galaxy (top row), elliptical galaxy (middle row), and irregular galaxy (bottom row). We find the minimum reconstruction error for $P_{\max}=45$ for spiral, elliptical, and irregular galaxies. For more or less value than 45, the reconstructed image deviated from the original image. In the case of minimal reconstruction error, we expect to well match objects, shapes, and their orientations or morphologies in reconstructed images and original images. ZPs include orthogonal functions; hence, moments give the properties of an image. Due to the Fourier term in the azimuthal angle function, the absolute value of moments is independent of the objects' rotation angle in the image. Space missions and ground base instruments observe solar features from various perspectives and scales. The Soho was in the first Lagrangian point of the Sun-Earth. STEREO A and B are in Earth's orbit. Figure 7 presents the ZMs of an active region observed by two STEREO A and B. The ZMs are similar from two different viewpoints. The block structures of the ZMs series are identical, with slight differences. These trivial differences may be due to the digital rather than the continuous image. Applying a transformation (to the image centre of brightness) and image normalization, ZMs will be translation and scaling invariances, respectively see, e.g., [41]

The SoHO/EIT and SDO/AIA resolutions are 0.6 and 2.4, respectively. The ZMs for the active region (Figure 8) with various resolutions are slightly similar. It seems the ZMs are functions of the morphology and geometry of the objects and depend less on the object's size.

4 Python code for ZMs

The Python code is available at GitHub (<https://github.com/hmddev1/ZEMO>) and PyPI (<https://pypi.org/project/ZEMO/1.0.0/>). The Python code calculates ZMs for a given

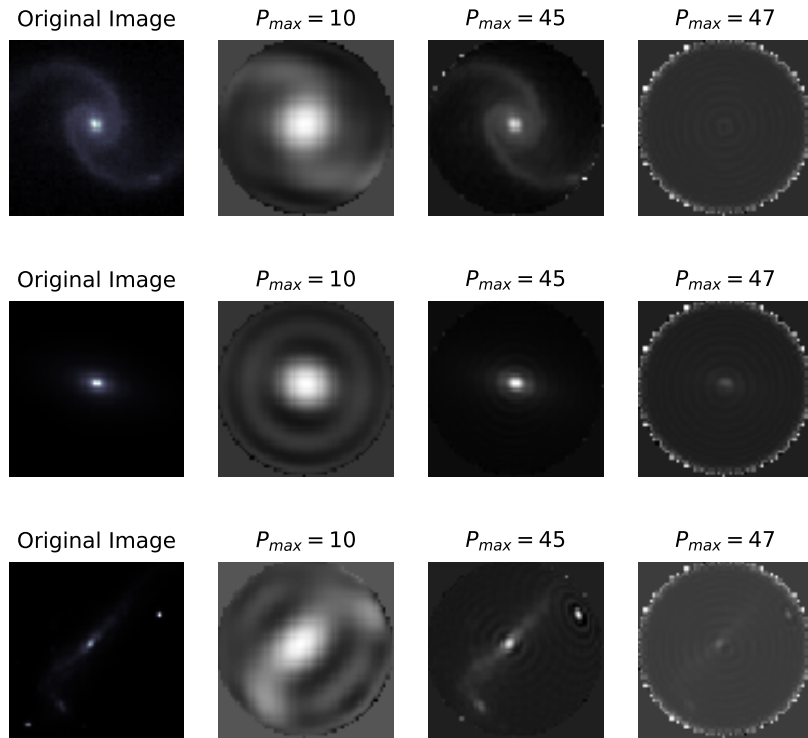


Figure 6: From left to right, panels represent the original and reconstructed images with the different maximum order numbers ($P_{max} = 10, 45, \text{ and } 47$), respectively, for a spiral galaxy (top row), elliptical galaxy (middle row), and irregular galaxy (bottom row). Recorded by SDSS survey.

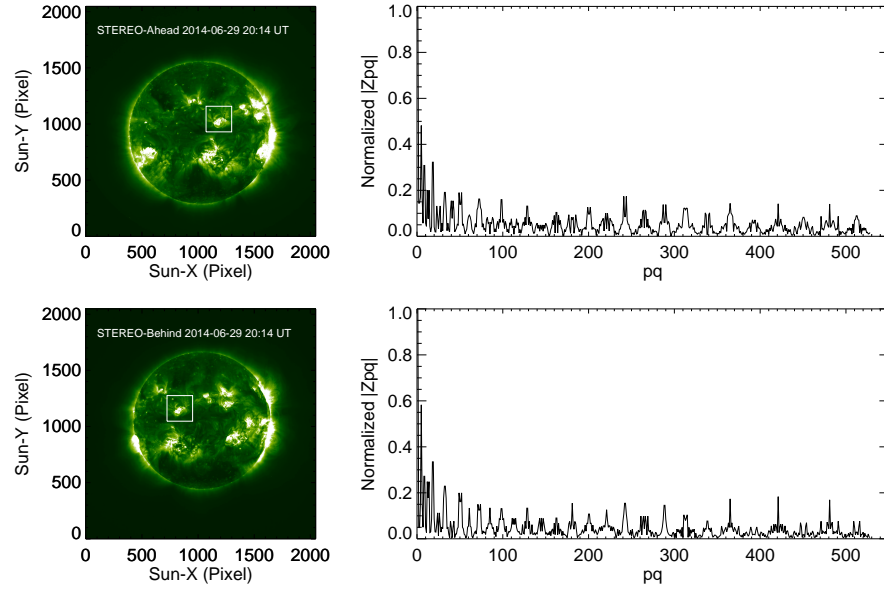


Figure 7: A solar active region indicated by a white box of the EUVI images at 195 Å recorded by STEREO-A (Left top) and STEREO-B (Left bottom). The normalized absolute values of the Zernike moments for $P_{\max}=31$ [38].

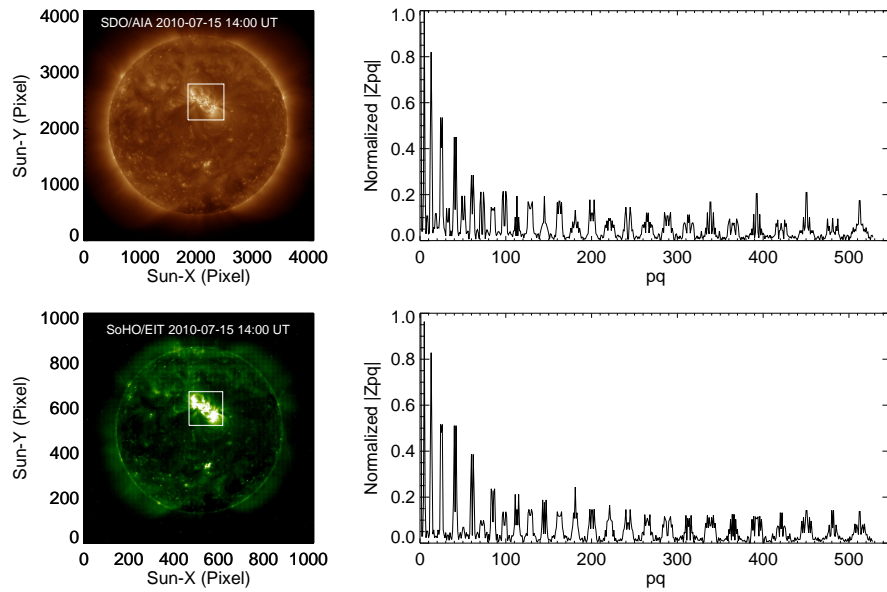


Figure 8: The white boxes represent of an active region observed by SDO/AIA image at 193 Å (Left top panel) and SoHO/EIT (Left bottom panel).(Right) The normalized absolute value of Zernike moments for two SDO and SoHo views [38].

image. [42] and [38] used the primitive code for calculating ZMs of solar features. The code includes the following functions:

- The `zernike_order_list` function calculates factorials, p (order numbers)-indices, and q (repetition numbers)-indices for a given maximum order number of Zernike polynomials.
- The `robust_fact_quot` function removes common elements from lists and calculates product quotients.
- The `zernike_bf` function generates Zernike basis functions stored in a complex-valued grid.
- The `zernike_mom` function calculates Zernike moments by summing the product of the image and basis functions.
- The `zernike_rec` function reconstructs an image by summing the weighted Zernike basis functions via ZMs.

The code includes checks for data validity, such as square image size matching, and prints informative error messages.

5 Conclusion

The Zernike polynomials indicate the distance along the radius and azimuthal angle. Equation (5) shows the image function weighted by the radial part $rR_{pq}(r)$. We note that $|R_{pq}(r)| < 1$ and $|rR_{pq}(r)| < r$ within a unit circle that shows that the edge's pixels have more extensive weights than the center pixels. The higher-order Zernike polynomials will show more oscillations to extract information on the image details along the radius from the origin to the perimeter [43].

Why are ZMs helpful in expressing an image?

- The Zernike basis is orthogonal and complete set functions, so ZMs are unique quantities features.
- We may reconstruct the original image by a finite number of moments.
- ZMs are slightly sensitive to noises.
- The magnitude of ZMs is rotation invariant. Image normalization makes translation and scale invariants for ZMs.

These reasons showed the capability of ZMs to describe an image to apply machine learning to identify and track the features in several disciplines. We published the Python code via GitHub and PyPI.

Acknowledgment

The authors would to thank NASA/SDO science group for making data publicly available.

Authors' Contributions

All authors have the same contribution.

Data Availability

The data used here are available at GitHub (<https://github.com/hmddev1/ZEM0>) and PyPI (<https://pypi.org/project/ZEM0/1.0.0/>)

Conflicts of Interest

The authors declare that there is no conflict of interest.

Ethical Considerations

The authors have diligently addressed ethical concerns, such as informed consent, plagiarism, data fabrication, misconduct, falsification, double publication, redundancy, submission, and other related matters.

Funding

This research did not receive any grant from funding agencies in the public, commercial, or nonprofit sectors.

References

- [1] Goshtasby, A. 1985, *IEEE Transactions on Pattern Analysis and Machine Intelligence*, 338.
- [2] Heywood, M., & Noakes, P. 1995, *IEE Proceedings-Vision, Image and Signal Processing*, 142, 213.
- [3] Aschwanden, M. J. 2010, *Solar Physics*, 262, 235.
- [4] Zheng, C., Pulido, J., Thorman, P., & Hamann, B. 2015, *Monthly Notices of the Royal Astronomical Society*, 451, 4445.
- [5] Moradkhani, M., Amiri, A., Javaherian, M., & Safari, H. 2015, *Applied Soft Computing*, 35, 123.
- [6] Noori, M., Javaherian, M., Safari, H., & Nadjari, H. 2019, *Advances in Space Research*, 64, 504.
- [7] Honarbakhsh, L., & Morra, G. 2023, *J. Geophysical Research (Solid Earth)*, 128, e2022JB025728.
- [8] Gonzaga, A., & Ferreira Costa, J. A. 1996, *Society of Photo-Optical Instrumentation Engineers (SPIE) Conference Series*, edited by Tescher, A. G. 2847, 223.
- [9] Teh, C.-H., & Chin, R. T. 1988, *Computer Vision and Pattern Recognition, Proceedings CVPR'88.*, Computer Society Conference on, IEEE.
- [10] Gonzalez, R., & Faisal, Z. 2019, *Digital Image Processing Second Edition*.
- [11] Hu, M.-K. 1962, *IRE Transactions on Information Theory*, 8, 179.

- [12] Flusser, J. 2000, *Pattern Recognition*, 33, 1405.
- [13] Nayak, D. R., Dash, R., & Majhi, B. 2018, *J. Med. Syst.*, 42, 1.
- [14] Zhang, Y., Wang, S., Sun, P., & Phillips, P. 2015, *Bio-medical materials and engineering*, 26, S1283.
- [15] Doerr, F., & Florence, A. 2020, *International Journal of Pharmaceutics: X*, 2.
- [16] Mukundan, R., Ong, S., & Lee, P. A. 2001, *IEEE Transactions on image Processing*, 10, 1357.
- [17] Mukundan, R., & Ramakrishnan, K. R. 1995, *Pattern Recognit.*, 28, 1433.
- [18] Belkasim, S., Ahmadi, M., & Shridhar, M. 1996, *J. the Franklin Institute*, 333, 577.
- [19] Zhenjiang, M. 2000, *Pattern Recognition Letters*, 21, 169.
- [20] Gu, J., Shu, H., Toumoulin, C., & Luo, L. 2002, *pattern Recognition in Information Systems*, 35, 2905.
- [21] Chong, C.-W., Raveendran, P., & Mukundan, R. 2003, *Pattern Recognition*, 36, 731.
- [22] Sim, D.-G., Kim, H.-K., & Park, R.-H. 2004, *Image and Vision Computing*, 22, 331.
- [23] Mitziias, D. A., & Mertzios, B. G. 2004, *Measurement*, 36, 315.
- [24] Papakostas, G. A., Boutalis, Y. S., Papaodysseus, C., & Fragoulis, D. K. 2006, *Image and Vision Computing*, 24, 960.
- [25] Papakostas, G. A., Boutalis, Y. S., Karras, D. A., & Mertzios, B. G. 2007, *Information Sciences*, 177, 2802.
- [26] Sadeghi, M., Javaherian, M., & Miraghaei, H. 2021, *AJ*, 161, 94.
- [27] Niu, K., & Tian, C. 2022, *J. Optics*, 24, 123001.
- [28] Capalbo, V., et al. 2022, *EPJ Web of Conferences*, 257, 00008.
- [29] Yousefzadeh, M., Safari, H., Attie, R., & Alipour, N. 2016, *Solar Physics*, 291.
- [30] Javaherian, M., Safari, H., Amiri, A., & Ziaei, S. 2014, *Solar Physics*, 289, .
- [31] Shokri, Z., et al. 2022, *ApJ*, 926, 42.
- [32] Hosseini Rad, S., Alipour, N., & Safari, H. 2021, *ApJ*, 906, 59.
- [33] Alipour, N., Safari, H., & Innes, D. E. 2012, *ApJ*, 746, 12.
- [34] Honarbakhsh, L., Alipour, N., & Safari, H. 2016, *Solar Physics*, 291, 941.
- [35] Alipour, N., et al. 2022, *A&A*, 663, A128.
- [36] Raboonik, A., Safari, H., Dadashi, N., & Alipour, N. 2016, 41st COSPAR Scientific Assembly.
- [37] Wheatland, M., Alipour, N., Raboonik, A., & Safari, H. 2017, *Institute of Physics Publishing*.

- [38] Alipour, N., Mohammadi, F., & Safari, H. 2019, *ApJS*, 243, 20.
- [39] Grubbström, R. W., & Tang, O. 2006, *European J. Operational Research*, 170, 106.
- [40] Wolf, C., et al., Technical report, Technical Report LIRIS. Available at <http://liris.cnrs.fr/Documents/Liris-5294.pdf> (unpublished).
- [41] Khotanzad, A., & Hong, Y. H. 1990, *IEEE Transactions on pattern analysis and machine intelligence*, 12, 489.
- [42] Alipour, N., & Safari, H. 2015, *ApJ*, 807, 175.
- [43] Shutler, J. D., & Nixon, M. S. 2001, *Proceedings of the British Machine Vision Conference*.